ORIENTAL JOURNAL OF CHEMISTRY
An International Open Access, Peer Reviewed Research Journal
www.orientjchem.org
ISSN: 0970-020 X
CODEN: OJCHEG
2025, Vol. 41, No.(1):
Pg. 57-65

Delving Ethyl 2-Oxo-2H-Chromene-3-Carboxylate as a Corrosion Inhibitor for Aluminum in Acidic Environments

APHOUET AURELIE KOFFI[1]*, SOULEYMANE COULIBALY[1], MAMADOU YEO[2], KAKARY KOLO COULIBALY[1] and PAULIN MARIUS NIAMIEN[1]

[1]*Université Félix Houphouët-Boigny, Abidjan-Cocody, 22 B.P. 582 Abidjan 22, Côte D' Ivoire.
[2]Université Nangui Abrogoua, 02 BP 802 Abidjan 02, Côte D' Ivoire.
*Corresponding author E-mail: koffiaphouet@yahoo.fr

http://dx.doi.org/10.13005/ojc/410106

(Received: December 04, 2024; Accepted: February 14, 2025)

ABSTRACT

Preserving metals by inhibiting corrosion is crucial; however, many traditional inhibitors are environmentally hazardous due to their toxicity and non-biodegradability. Therefore, this study proposes ethyl 2-oxo-2*H*-chromene-3-carboxylate as an eco-friendly corrosion inhibitor. The analysis was carried out on aluminum in a hydrochloric acid molar solution using gravimetry and Density Functional Theory (DFT). The findings revealed that ethyl 2-oxo-2*H*-chromene-3-carboxylate exhibited significant inhibition with an efficiency of 90.5% at a concentration of 5.10^{-4} M at 45°C. The adsorption behavior followed the Temkin model, indicating favorable surface interactions. Additionally, a lower activation energy in the inhibited medium and endothermic dissolution of aluminum, as indicated by the calculated thermodynamic parameters, suggest chemical adsorption. DFT calculations revealed a negative fraction (ΔN = -0.153 *eV*), indicating that chemisorption was facilitated by electron transfer from the 3s orbital of aluminum to ethyl 2-oxo-2H-chromene-3-carboxylate. Frontier orbital analysis highlighted active sites at O16, C9, and C13 atoms, supporting the mechanisms of molecular adsorption.

Keywords: Corrosion inhibition, Ethyl 2-oxo-2*H*-chromene-3-carboxylate, Aluminum, Hydrochloric acid.

INTRODUCTION

Corrosion can be defined as the process in which materials are destroyed when interacting with an aggressive environment[1]. The damages caused by corrosion depend on the temperature, pressure, pH, and type of corrosive medium. Temperature in particular plays an important role in the formation of protective barriers on metal surfaces. The corrosion of materials remains a pervasive issue, resulting in substantial annual losses across various industries[2-4]. In addition to its economic impact, corrosion contributes to environmental degradation and poses a risk to human health. In industrial settings, corrosion induced by acidic solutions often requires the incorporation of organic compounds into the medium to mitigate the degradation[5,6]. Highly acidic environments, like hydrochloric, sulfuric, and phosphoric acid are commonly used in various industrial cleaning processes, including cleaning oil wells, removing scale, and treating metals.

Recent research efforts have focused on developing eco-friendly and sustainable inhibitors derived from natural sources, aiming to minimize environmental impact while maintaining high efficacy in corrosion prevention[7-14]. These green inhibitors include glutaraldehyde (HC=O), azo derivatives (N=N), hydrazones (C=N–N), and azol compounds (heterocyclic compounds containing a nitrogen atom). Other researchers have investigated three chromeno-carbonitrile derivatives for their effectiveness as corrosion inhibitors[15]. These molecules have many functional groups and aromatic rings and provide good protection against corrosion. The results revealed that the inhibition efficiencies follow the sequence INH-1<INH-2<INH-3 with values of 89.16%, 93.02%, and 95.32% at a concentration of 10^{-3} M in one molar hydrochloric acid. Similarly, Larioui *et al.,* synthesized two chromen-6-one derivatives (BCC-Ph and BCC-Fur) to inhibit mild steel corrosion in the same medium[16]. Tigori *et al.,* have also studied the inhibitory properties of a chromene derivative in an acidic environment[17]. This inhibitor achieved an inhibition efficiency of 92.20% at a concentration of 2×10^{-4} M.

The organic inhibitors contain high electron density centers (heteroatoms and π bonds) that facilitate adsorption on metal surfaces and provide protection against corrosive environments. They can get adsorbed physically, chemically, or by both types of adsorption. The inhibitor's capacity to adsorb onto the surface of a substrate is influenced by electrolyte type, surface charge, and working conditions[18,19]. Interactions within the metal-inhibitor interface can be elucidated using adsorption isotherms, thermodynamic parameters, and quantum chemical calculations[15,19].

In line with this, our study investigated the potential of ethyl 2-oxo-2*H*-chromene-3-carboxylate, an organic molecule belonging to the chromene family, as a corrosion inhibitor. Chromenes are heterocyclic systems with a phenyl ring fused to an oxine ring. Notably, this compound has already been utilized in anticorrosion lubricants, paints, and coatings, underscoring its potential efficacy[20]. To the best of our knowledge, this compound has not yet been studied in an acidic environment and therefore constitutes the novelty of this study.

Ethyl 2-oxo-2*H*-chromene-3-carboxylate is typically synthesized through a reaction between salicylic acid and acetic anhydride, with the final product isolated via recrystallization, underscoring its promising avenue for corrosion inhibition. Indeed, this molecule contains functional groups such as–COO and aromatic rings through which adsorption can occur, and the adsorption process is essential for the inhibitory effectiveness of a compound[21].

This study seeks to comprehensively examine the inhibition behavior of ethyl 2-oxo-2*H*-chromene-3-carboxylate on aluminum corrosion in an acid medium using a combination of experimental and theoretical techniques. Evaluation of the inhibition efficiency was conducted through mass-loss measurements. At the same time, thermodynamic parameters and quantum chemical calculations helped to lighten the underlying inhibition mechanism and assess the influence of temperature on inhibition efficiency.

MATERIALS AND METHODS

Aluminum samples and electrolyte medium

High-purity aluminum rods (99.6%) were precisely cut into 1 cm lengths and subjected to meticulous pre-treatment to eliminate any residual impurities. During pre-treatment, the samples were polished with abrasive paper, cleaned with acetone solution and distilled water; and then oven-dried at 343 K for 10 minutes[22]. Subsequently, the aluminum rods were immersed in the electrolyte solution. The inhibitor concentrations ranged from 10^{-4} to 5×10^{-4} M, allowing for a comprehensive assessment of its inhibitory efficacy. Each sample was subjected to immersion for one hour to ensure adequate exposure to the corrosive environment and the effects of the inhibitor.

Synthesis and inhibitor elaboration

The chemical reagents and solvents were from Sigma Aldrich and used without further purification. TLC analyses were conducted on silica gel plates (Sorbent Silica G UV254). Column chromatography was carried out on flash silica gel (Sorbent 230–400 mesh). NMR ^{1}H and ^{13}C NMR spectra were recorded at 500 and 126 MHz, respectively, in $CDCl_3$ solution provided by Eurisotop, using TMS as an internal reference on a Bruker instrument. Coupling constants (J) and

chemical shifts (δ) are given in hertz and ppm respectively, using TMS as internal standards. Multiplicities are denoted as s (singlet), d (doublet), dd (doublet of doublet), t (triplet), q (quartet), m (multiplet), and coupling constants (J) are reported in Hz. The compound under investigation is ethyl 2-oxo-2*H*-chromene-3-carboxylate (Fig. 1) with chemical formula $C_{12}H_{11}O_4$ and molar mass M = 218.207 g.mol^{-1}.

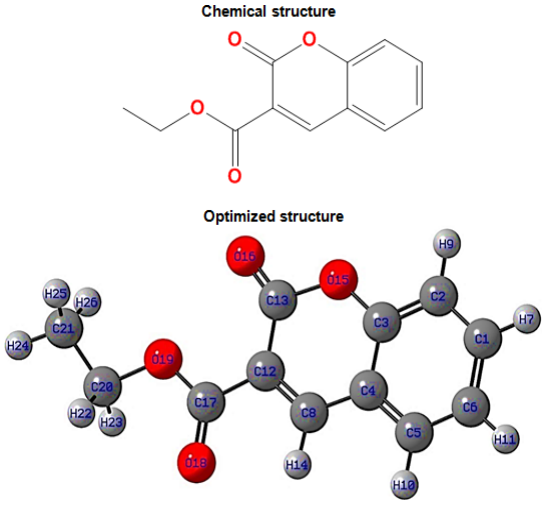

Fig. 1. Ethyl 2-oxo-2H-chromene-3-carboxylate

It was synthesized following the procedure outlined by Alvin *et al.,*[23]. 5 mL of salicylic aldehyde (47.9 mmol; 1 eq), 9.5 mL of ethyl malonate (6.23 mmol; 1.3 eq), and piperidine (400 µL) were combined into a Bicol. The mixture was magnetically stirred at room temperature. After 30 min, the reaction was monitored by thin-layer chromatography (TLC). Subsequently, the reaction mixture was neutralized using hydrochloric acid solution. This resulted in a residue purified by chromatography on silica gel using an 80/20 hexane/ethyl acetate as eluent system. The final product was obtained in 94% yield and characterized using ^{1}H and ^{13}C nuclear magnetic resonance (NMR) spectroscopy. ^{1}H NMR (500 MHz, $CDCl_3$) (δ ppm): 8.51 (s ; 1H ; H4); 7.64 (t ; *J* = 7.2 Hz ; 1H ; H7) ; 7.61 (d ; *J* = 7.8 Hz ; 1H ; H5) ; 7.34 (t ; *J* = 7.8 Hz ; 1H ; H6) ; 7.31 (d ; *J* = 1.3 Hz ; 1H ; H8) ; 4.41 (q ; *J* = 7.2 Hz ; 2H ; -CH_2) ; 1.40 (t ; *J* = 7.2 Hz ; 3H ; -CH_3). ^{13}C NMR (126 MHz, $CDCl_3$) (δ ppm): 163.21; 156.81; 155.33 ; 148.66 ; 134.43 ; 129.61 ; 124.95 ; 118.55 ; 118.04 ; 116.93 ; 62.11 ; 14.36.

Study by gravimetric method

The aluminum degradation rate and the tested molecule's effectiveness were assessed by quantifying the mass loss incurred by one hour of exposure in the electrolyte medium across a range of temperatures (308-318 K). The corrosion rate *CR* (g. cm^{-2}. h^{-1}) was assessed by Equation (1) in which Δm represents the mass loss (g) ; *S* denotes the specimen's surface (cm^2) ; and *t* represents the immersion time (h).

$$CR = \Delta m/(S \times t) \quad (1)$$

The effectiveness of inhibition IE(%) was calculated according to the expression below:

$$IE = (CR_0\text{-}CR)/CR_0 \times 100 \quad (2)$$

Here, CR_0 and CR represent the corrosion rates in the absence and presence of the inhibitor, respectively.

Theoretical analysis by density functional theory calculation

Computations in quantum chemistry were performed to investigate the chemical properties of ethyl 2-oxo-2*H*-chromene-3-carboxylate. Initially, the molecular structure was sketched and pre-optimized using GaussView 5.0.8. Subsequently, computations were carried out employing Gaussian 09 W software. In this program, the DFT/B3LYP method with the 6-311 G basis set was applied[23,24]. The energy of the highest occupied molecular orbital (E_{HOMO}) and the lowest unoccupied molecular orbital (E_{LUMO}) were obtained. Then, the chemical potential (μ), the hardness (η), the softness (S), the electronegativity (χ), and the electrophilicity index (ω) were deduced.

RESULTS AND DISCUSSION

Exploration of corrosion inhibition of aluminum

The corrosion rate of the aluminum samples was assessed both in the HCl blank solution and in the presence of ethyl 2-oxo-2*H*-chromene-3-carboxylate. As depicted in Fig. 2, CR decreased from 0.0034 g.cm^{-2}. h^{-1} to 0.0015 g.cm^{-2}.h^{-1} at 308K. An identical trend occurred at 313K and 318K. This finding highlights the inhibitory effect of the molecule investigated in a 1 M hydrochloric acid medium. Besides, the results revealed a significant increase in substrate dissolution as the temperature increased.

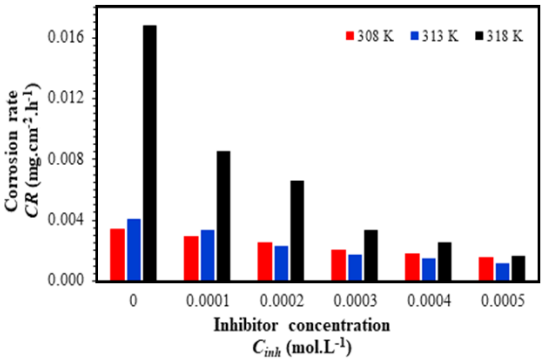

Fig. 2. Plots of Corrosion rate (CR) versus ethyl 2-oxo-2*H*-chromene-3-carboxylate concentration (Cinh), in the temperature range 308K-318K

This increase in the corrosion rate can be attributed to thermal agitation, which facilitates the accelerated movement of reactants across the energy barrier[25,26]. However, addition of ethyl 2-oxo-2*H*-chromene-3-carboxylate to the corrosive medium reduced the corrosion rate. A noticeable reduction in metal dissolution was observed at all the tested temperatures.

The inhibitory properties of ethyl 2-oxo-2*H*-chromene-3-carboxylate were evaluated by measuring its inhibition rate. As shown in Fig. 3, IE increased with inhibitor mass. Additionally, the molecule's effectiveness improved with increasing temperature up to 90.51%, which is attributed to the chemical adsorption of the inhibitory species[8].

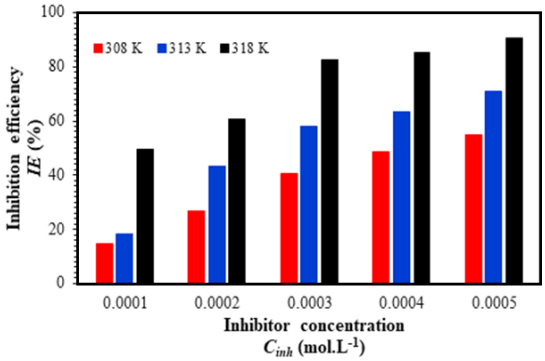

Fig. 3. Plots of Inhibition efficiency (IE) versus ethyl 2-oxo-2*H*-chromene-3-carboxylate concentration (Cinh), in the temperature range 308K-318K

Investigation of adsorption isotherms

In an acidic environment, a chemical species exerts its inhibitory effect by adsorbing onto the surface of the metal to be protected[9,10]. The interactions occurring during the adsorption process can be modeled. Three distinct models were investigated: Langmuir, Temkin, and El-Awady isotherms, described by Equations (3), (4) and (5) respectively[27-29].

$$C_{inh} / \theta = 1 / K_{ads} + C_{inh} \quad (3)$$

$$\theta = - (2.303 \log K)/2\alpha - (2.303 \log C_{inh})/2\alpha \quad (4)$$

$$\log (\theta/(1-\theta)) = y \log C_{inh} + \log K \quad (5)$$

The metal's surface coverage rate (θ) was used to determine which isotherm best describes the adsorption process over the temperature range 308 to 318K (Fig. 4). The fitting lines exhibited coefficients of determination (R-squared) approaching unity (Table 1).

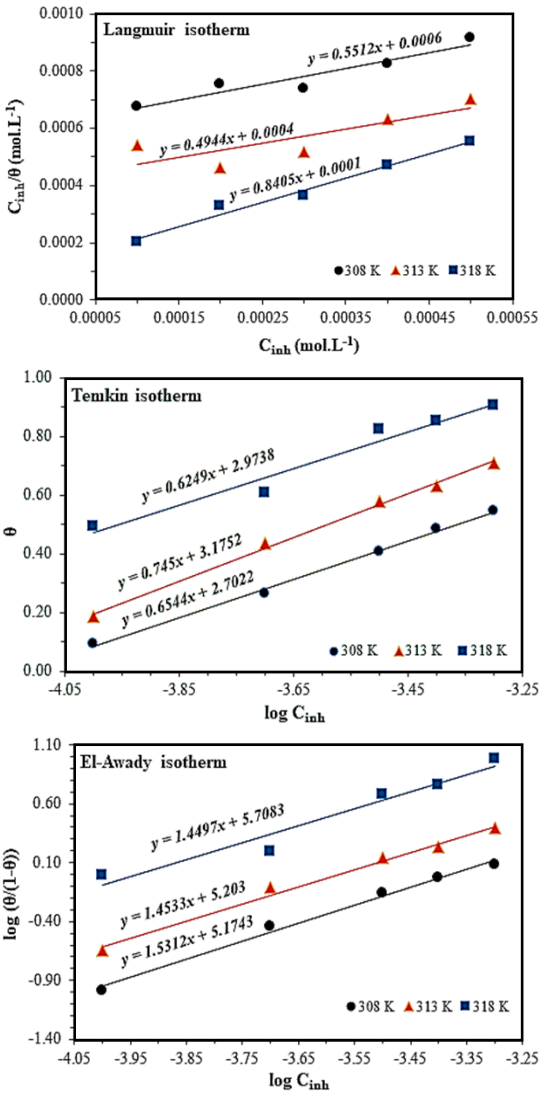

Fig. 4. Modeling of the adsorption of ethyl 2-oxo-2*H*-chromene-3-carboxylate molecule on aluminum surface

Table 1: Isotherm parameters

Isotherm	Parameters	308K	313K	318K
Langmuir	R^2	0.905	0.656	0.980
	K_L (L.mol^{-1})	919	1236	8405
Temkin	R^2	0.997	0.996	0.961
	A	-0.57	-0.65	-0.54
	K_T (L.mol^{-1})	13490	18197	57544
El-Awady	R^2	0.992	0.990	0.948
	1/y	0.65	0.69	0.69
	$K_{(E-A)}$	107.9	107.6	108.3

The Temkin isotherm provided the best fit, with R^2 values close to unity, showing that this model most accurately describes the adsorption of ethyl 2-oxo-2*H*-chromene-3-carboxylate onto the aluminum surface in a 1M HCl medium. Further analysis of the parameters of the different isotherms revealed the presence of repulsive interactions between adsorbed species, non-uniform distribution of adsorption sites on the metal surface, potential multilayer adsorption, and variation in adsorption energy with increasing surface coverage[30-33].

Analysis of the impact of temperature

Temperature variation induced corrosion rate was used in this study to determine key thermodynamic parameters of adsorption. These parameters include free enthalpy (ΔG_{ads}), enthalpy (ΔH_{ads}) and entropy (ΔS_{ads}). The Kads values were obtained from the Temkin model above and used to determine ΔG_{ads} (Equation 6). Subsequently, ΔH_{ads} and ΔS_{ads} were deduced from the plot of ΔG_{ads} versus T (Equation 7). Table 2 presents the results.

$$\Delta G_{ads} = - RT \ln (-55.5 \times \Delta K_{ads}) \quad (6)$$

$$\Delta G_{ads} = \Delta H_{ads} - T\Delta S_{ads} \quad (7)$$

55.5 represents the molar concentration of water.

Table 2: Adsorption parameters of ethyl 2-oxo-2*H*-chromene-3-carboxylate adsorption onto aluminum surface

T(K)	ΔG_{ads} (kJ.mol^{-1})	ΔH_{ads} (kJ.mol^{-1})	ΔS_{ads} (J.mol-1.K^{-1})
308	- 34.62	143.38	554.60
313	- 35.97		
318	- 39.57		

ΔG_{ads} is negative, hinting that the adsorption of ethyl 2-oxo-2*H*-chromene-3-carboxylate species on the aluminum surface is spontaneous. Furthermore, the values range between–39.57 kJ.mol^{-1} and –34.62 kJ.mol^{-1}, suggesting that the adsorption process involves both physical and chemical interactions[34,35]. Positive values of ΔH_{ads} point to an endothermic process associated with chemisorption[36,37]. These results confirmed that ethyl 2-oxo-2*H*-chromene-3-carboxylate underwent chemical adsorption on the metal surface. The positive change in adsorption entropy implies an increase in disorder within the solution during the adsorption process[39,40]. Moreover, the adsorption of inhibitory species in an aqueous medium is associated with water molecules desorbed at the substrate surface, as illustrated by chemical equilibrium {1}.

$$Inh_{(sol)} + n\ H_2O_{ads} \longrightarrow Inh_{ads} + n\ H_2O_{(sol)} \quad \{1\}$$

Analysis of activation parameters

The adsorption phenomenon was also investigated by plotting log CR and log (CR/T) versus 1000/T using the Arrhenius relation (Equation 8) and the transition state relation (Equation 9). This is translated into the activation energy (E_α*) as well as the changes in enthalpy (ΔH_α*) and entropy (ΔS_α*) of activation indicated in Table 3.

$$CR = A \times \exp (- E_\alpha^* / (2.3\ R.T)) \quad (8)$$

$$CR = \exp (\Delta S_a^*/R) \times \exp (-(\Delta H_a^*/(R.T)) \times (R.T)/(\aleph.h) \quad (9)$$

Table 3: Activation parameters of ethyl 2-oxo-2*H*-chromene-3-carboxylate adsorption onto aluminum surface

C_{inh} (10^{-4} mol.L^{-1})	E_α* (kJ.mol^{-1})	ΔH_α* (kJ.mol^{-1})	ΔS_α* (J.mol^{-1}K^{-1})
0	129.439	126.838	512.729
1	82.217	79.616	359.101
2	78.471	75.870	344.828
3	29.788	27.187	185.606
4	28.491	25.890	180.265
5	2.505	-0.096	94.961

Remarkably, in this study, the activation energy for aluminum corrosion was higher in the blank solution. However, it is reported that when adding an inhibitor in an acidic medium, if E_a* increases, it could be attributed to physisorption, whereas chemisorption typically results in decreased Ea*[33,36]. This observation therefore suggests that a chemical reaction occurred between the metal surface and the adsorbed molecule.

The positive values of ΔH_a* indicate that

the dissolution of aluminum in the HCl medium is an endothermic process[33]. Moreover, the positive value of ΔS_a^* suggests that the activated complex follows a dissociative mechanism, resulting in increased disorder. This phenomenon occurs because in the transition state, the activated complex is weakly bound and approaches dissociation[34,41]. Furthermore, the adsorption of ethyl 2-oxo-2*H*-chromene-3-carboxylate can be viewed as the substitution of water molecules by the inhibitor species, further contributing to the increased disorder in the inhibited medium[36].

DFT analysis

Quantum chemical calculations were carried out to explore the inhibition mechanism of ethyl 2-oxo-2*H*-chromene-3-carboxylate. The geometry optimization of the molecule under investigation is illustrated in Fig. 5, and Tables 4 and 5 provide a comprehensive overview of the obtained results.

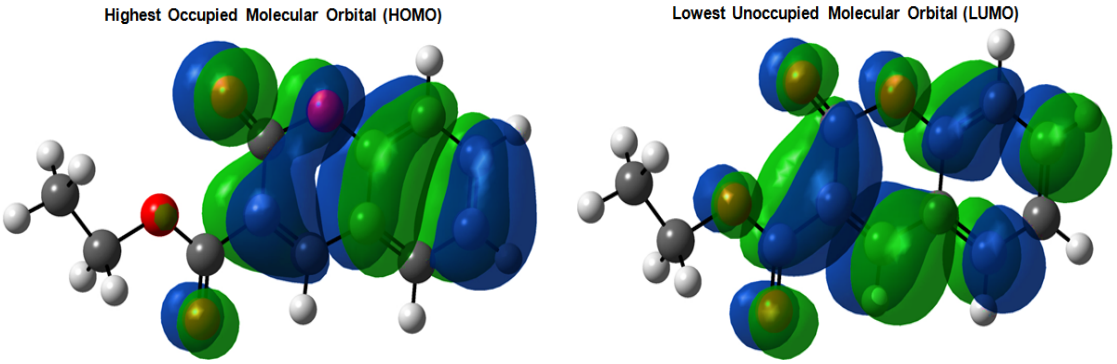

Fig. 5. Frontier orbitals of ethyl 2-oxo-2*H*-chromene-3-carboxylate

Table 4: Global reactivity descriptors of ethyl 2-oxo-2H-chromene-3-carboxylate

E_{HOMO}(eV)	E_{LUMO}(eV)	ΔE(eV)	μ(D)	E_T(ua)	χ(eV)	η(eV)	S(eV^{-1})	ω(eV)	ΔN
-7.019	-2.822	4.197	3.75	-764.17	4.921	2.098	0.477	5.769	-0.153

As shown in Fig. 5, the electron densities of HOMO and LUMO are primarily concentrated around the aromatic rings and oxygen atoms of the molecule. Therefore, the active sites of the molecule are likely to be located at oxygen and carbon atoms. Further insights into the reactivity of the molecule are provided by Fukui functions, which identify the sites prone to electrophilic and nucleophilic attacks. The molecular global reactivity descriptors (Table 4) indicate that E_{HOMO} and E_{LUMO} values are consistent with the literature[42-45]. The notably high value of E_{HOMO} suggests the molecule's tendency to donate electrons, whereas a relatively low value of E_{LUMO} indicates its ability to accept electrons. Additionally, the electronegativity χ of a molecule reflects its capacity to attract electrons. Our study found that the theoretical electronegativity value (3.850 *eV*) is comparatively low relative to the work function of aluminum Φ_{Al} (Φ_{Al} = 4.28 eV)[46]. Consequently, the fraction of electrons transferred is negative (ΔN = -0.153 *eV*) indicating that the inhibitor species can accept electrons from the metal[47]. Similarly, the high electrophilicity index (ω = 5.769 *eV*) reinforces the electrophilic nature of the studied molecule[48,49], thereby corroborating the observed chemisorption (vide supra). Furthermore, the electronic gap ΔE is an indicator of the molecule's chemical reactivity. In this case, a relatively low ΔE = 4.197 *eV* suggests favorable interactions between the molecule and other species in the medium, particularly with the metal surface[50].

The active zones of the molecule were selected using Fukui functions (f_k^+, f_k^-) and the dual index (Δf_k), as defined by the following equations:

$$f_k^+ = q_k (N+1) - q_k (N) \quad (10)$$

$$f_k^- = q_k (N) - q_k (N - 1) \quad (11)$$

Here, q_k (N+1), q_k (N) and q_k (N - 1) are the electronic populations of the atom k in the anionic, neutral, and cationic forms, respectively.

$$\Delta f_k = f_k^+ - f_k^- \quad (12)$$

Where f_k^- and f_k^+ denote the electrophilic and nucleophilic attack sites, respectively.

Table 5: Fukui functions and dual descriptor of pertinent atoms of ethyl 2-oxo-2H-chromene-3-carboxylate

Atom N°	q_k(N-1)	q_k(N)	q_k(N+1)	f_k^-	f_k^+	Δf_k
C1	-0.146	-0.105	-0.070	0.041	0.035	-0.006
C2	-0.193	-0.149	-0.099	0.044	0.05	0.006
C3	0.234	0.273	0.317	0.039	0.044	0.005
C4	-0.030	-0.081	-0.075	- 0.051	0.006	0.057
C5	-0.134	-0.082	-0.049	0.052	0.033	-0.019
C6	-0.185	-0.174	-0.128	0.011	0.046	0.035
C9	-0.114	-0.020	0.017	0.094	0.037	-0.057
C12	-0.269	-0.279	-0.250	- 0.010	0.029	0.039
C13	0.478	0.539	0.546	0.061	0.007	-0.054
O15	-0.563	-0.518	-0.452	0.045	0.066	0.021
O16	-0.387	-0.298	-0.154	0.089	0.144	0.055
C17	0.445	0.503	0.562	0.058	0.059	0.001
O18	-0.484	-0.399	-0.342	0.085	0.057	-0.028
O19	-0.482	-0.454	-0.455	0.028	-0.001	-0.029
C20	-0.078	-0.110	-0.125	- 0.032	-0.015	0.017
C21	-0.521	-0.521	-0.524	0	-0.003	-0.003

Sites susceptible to nucleophilic attack exhibit positive values of f_k^+ and the highest values of Δf_k, whereas those prone to electrophilic attack possess positive values of f_k^- and the most negative dual descriptor[47,51]. In our investigation (Table 5), the atoms C4, and O16 of ethyl 2-oxo-2*H*-chromene-3-carboxylate were identified as potential nucleophilic attack sites. However, the oxygen atom O16 is the most likely site, with Δf_k = 0.055. Conversely, atom C4 despite having the highest dual index value (Δf_k = 0.057) is less likely to be a preferential attack site due to its lower electron deficiency. According to Table 5, atoms C9 and C13 are predicted to be primary sites for electrophilic attack, as they exhibit the most negative Δf_k values. These predicted attack sites correspond well to the characteristics of the frontier molecular orbitals.

Proposed inhibition mechanism

Protection of metal against corrosion in acidic environments arises from the adsorption of neutral or cationic species onto the metal surface[52,53]. The cationic form is obtained by protonation of the inhibitor. This adsorption is facilitated by interactions such as lone-pair electrons and π bonds. Consequently, the extent of adsorption is governed by various factors, including the charge on the substrate, the inhibitor's structure, and the electrolyte. This adsorption process is generally put into physisorption and chemisorption[54].

As illustrated in Fig. 6, the adsorption of ethyl 2-oxo-2*H*-chromene-3-carboxylate on the aluminum surface was of a mixed type.

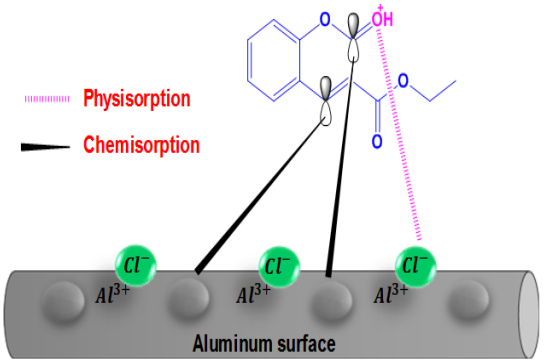

Fig. 6. Mechanism of adsorption of ethyl 2-oxo-2*H*-chromene-3-carboxylate on aluminum surface

Chemisorption results from the ethyl 2-oxo-2*H*-chromene-3-carboxylate molecule forming bonds with the aluminum surface by accepting electrons from the metal's 3s orbitals, confirmed by the negative ΔN parameter. In addition, ethyl 2-oxo-2*H*-chromene-3-carboxylate undergoes protonation in an acidic environment. According to the DFT protonation of the molecule would occur on the oxygen atom O16, leading to the cations shown in Fig. 7. These cations can interact with the aluminum surface primarily governed by the chloride ions. In fact, Cl^- ions are attracted to Al^{3+} ions formed at the substrate surface due to corrosion. The adsorbed Cl^- ions then facilitate the adsorption of the protonated inhibitor, thus slowing down the loss of the metal. The interaction between protonated ethyl 2-oxo-2*H*-chromene-3-carboxylate and the negatively charged aluminum surface is physical.

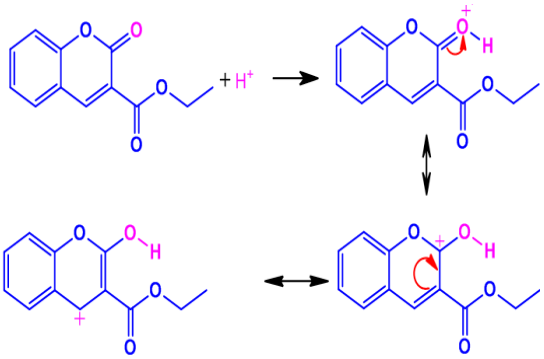

Fig. 7. Proposed mechanism for protonation of ethyl 2-oxo-2*H*-chromene-3-carboxylate based on DFT results

Protonated inhibitors can also compete with H^+ ions at cathodic sites on metal surfaces[55]. The electrons formed during metal oxidation negatively charged the metal surface, promoting the attraction

of the cation inhibitor. Electrostatic forces primarily govern interactions between protonated species and metal surface. Furthermore, aluminum corrosion can be inhibited through the physical adsorption of metal complexes formed between ethyl 2-oxo-2*H*-chromene-3-carboxylate molecules and Al^{3+} ions released in the HCl solution[52].

CONCLUSION

This study investigated the behavior of ethyl 2-oxo-2*H*-chromene-3-carboxylate as a corrosion inhibitor of aluminum in 1 M HCl medium. Experimental and theoretical methods were used to explore the effectiveness of this compound. Gravimetric analysis revealed that adding this compound to the acid solution significantly reduced aluminum dissolution, confirming its inhibitory properties. The efficiency of the inhibitor increased at both higher concentrations from 10^{-4} M to 5.10^{-4} M and with the rise in temperature from 308K to 318K, achieving an inhibition efficiency of 90.5%. The adsorption behavior followed the Temkin model, suggesting repulsive interactions and multilayer formation on the aluminum surface. Further analysis of the thermodynamic parameters suggested a mixed-type adsorption mechanism, facilitated by the presence of oxygen atoms and π bonds in the molecule.

Theoretical calculations using the DFT technique provided additional understanding of the molecular behavior, highlighting the location of the HOMO and LUMO orbitals and suggesting high reactivity due to a low energy gap. Fukui function analysis identified atoms C9 and C13 as potential sites for electrophilic attack and atom O16 as a likely site for nucleophilic attack. The negative fraction of electron transfer (ΔN = -0.153 *eV*) indicates that electrons are transferred from the metal surface to the ethyl 2-oxo-2*H*-chromene-3-carboxylate molecule, supporting the notion of chemical adsorption.

Overall, this study provides a comprehensive understanding of how ethyl 2-oxo-2*H*-chromene-3-carboxylate functions as a corrosion inhibitor. These insights could lead to the development of more effective corrosion prevention strategies for aluminum in aggressive environments. The combined experimental and theoretical approach not only confirmed the effectiveness of the compound but also detailed the underlying mechanisms of its inhibitory action.

ACKNOWLEDGMENT

No funding was received during this research work.

Conflict of interest

The authors reported no potential conflict of interest.

REFERENCES

1. Khormali, A.; Ahmadi, S., *Iran. J. Chem. Chem. Eng.*, **2023**, *42*(1), 321-336.
2. Ahmed, Al-A.; Wan, N. R. W. I.; Waleed, K. Al-A., *Ain Shams Eng. J.*, **2024**, *15*, 102672.
3. Aljibori, H. S.; Alamiery, A.; Kadhum, A. A. H., *Int. J. Corros. Scale Inhib.*, **2023**, *12*(4), 1476–1520.
4. Kania, H., *Coatings.*, **2023**, *13*(2), 216.
5. Yang, H.-M., *Molecules.*, **2021**, *26*(11), 3473.
6. Abbas, A.; Adesina, A. Y.; Suleiman, R. K., *Metals.*, **2023**, *13*, 1479.
7. Husaini, M.; Yunusa, U.; Ibrahim, H. A.; Usman, B.; Ibrahim, M. B., *Alg. J. Chem. Eng.*, **2020**, *01*, 12–21.
8. Khamaysa, O. M. A.; Selatnia, I.; Zeghache, H.; Hassane, L.; Sid, A.; Chung, I.-M.; Benahmed, M.; Gherraf, N.; Mosset, P., *J. Mol. Liq.*, **2020**, *315*, 113805.
9. Annon, I. A.; Abbas, A. S.; Al-Azzawi, W. K.; Hanoon, M. M.; Alamiery, A. A.; Isahak, W. N. R. W.; Kadhum, A. A. H. S., *Afr. J. Chem. Eng.*, **2022**, *41*, 244–252.
10. Ghaderi, M.; Ahmad, R. S. A.; Kordzadeh, A.; Mahdavian, M.; Alibakhshi, E.; Ghaderi, A., *Sci. Rep.*, **2022**, *12*, 13450.
11. Dyari, M. M.; Yousif, H. A.; Askander, K. K.; Karzan, M. A.; Rebaz, A. O.; Lana, O. A., *Comput. Theor. Chem.*, **2024**, *1237*, 114645.
12. Omer, R. A.; Koparir, P.; Koparir, M., *Prot. Met. Phys. Chem. Surf.*, **2023**, *59*, 1315–1325.
13. Mamad, D. M.; Rebaz, A. O.; Khdir, O. A., *Corros. Rev.*, **2023**, *41*(6), 703-717.
14. Mamad, D. M.; Rasul, H. H.; Awla, A. H.; Rebaz, A. O., *Dokl. Phys. Chem.*, **2023**, *511*, 125–133.
15. Quadri, T. W.; Alfantazi, A.; Obot, I. B.; Olasunkanmi, L. O.; Akpan, E. D.; Verma, C.; Al-Mohaimeed, A. M.; Ebenso, E. E.; Quraishi, M. A., *RSC Adv.*, **2021**, *11*, 2462.

16. Larioui, A.; Chaouki, I.; Hmada, A.; El Magri, A.; Errahmany, N.; El Hajri, F.; Dkhireche, N.; El Bakkali, S.; Touir, R.; Boukhris, S., *Mor. J. Chem.,* **2024**, *12*(2), 570-593.
17. Tigori, M. A.; Koné, A.; Souleymane, B.; Zon, D.; Sissouma, D.; Niamien, P. M., *Open J. Phys. Chem.*, **2022**, *12*, 47-70.
18. Wang, L.; Wang, H.; Seyeux, A.; Zanna, S.; Pailleret, A.; Nesic, S.; Marcus, P., *Corros. Sci.*, **2023**, *213*(1), 110952.
19. Betti, N.; Al Amiery, A. A.; Al Azzawin, W. K.; Isahak, W. N. R. W., Sci. Rep., 2023, 13, 8979.
20. Manal, M. K.; Nahla, A. T.; Aminah, A. B.; Ahmed, A. E.; Mai, S.; Nazli, H., *Alex. Eng. J.*, **2022**, *61*, 6397-6948.
21. Yan, L.; Qiao, X.; Wang, S.; Zhang, J.; Zhang, H., *J. Chem. Res.*, **2017**, *41*, 266-270.
22. Koffi, A. A.; Allou, N.B.; Tigori, M. A.; Teminfolo, Y. S.; Trokourey, A.; Niamien, P. M., *Eur. J. Chem.*, **2023**, *14*, 353-361.
23. Ogunyemia, B. T.; Latonab, D. F.; Ayindec, A. A.; Adejoro, I. A., *Adv. J. Chem.-Section A.,* **2020**, *3*(4), 485–492.
24. Quan, B.; Li, J.; Chen, C., *ACS Omega.*, **2021**, *6*, 25904–25915.
25. Okewale, A. O.; Adesina, O. A., *J. Appl. Sci. Environ. Manage.*, **2020**, *24*, 37-47.
26. Bouhlal, F.; Labjar, N.; Abdoun, F.; Mazkour, A.; Serghini-Idrissi, M.; El Mahi, M.; Lotfi El, M.; Hajjaji, S. El., *Int. J. Corr.,* **2020**, 4045802, 1-14.
27. Vimala, M.; Chandrasekaran, V., *Orient. J. Chem.*, **2023**, *39*(4), 1002-1006.
28. Akinbulumo, O. A.; Odejobi, O. J.; Odekanle, E. L., *Res. Mater.*, **2020**, *5*(1), 100074.
29. Andoor P.A., Okeoma K.B., Mbamara U.S., *Int. J. Phys. Sci.*, **2021**, *16*(2), 79-95.
30. Alahiane, M.; Oukhrib, R.; Albrimi, Y. A.; Oualid, H. A.; Bourzi, H.; Akbour, R. A.; Assabbane, A.; Nahlé, A.; Hamdan, M., *RSC Adv.*, **2020**, *10*, 41137–41153.
31. Samide, A.; Dobritescu, A.; Tigae, C.; Spînu, C. I.; Oprea, B., *Molecules.*, **2023**, *28*, 6799.
32. Méndez, C. M.; Gervasi, C. A.; Pozzi, G.; Ares, A. E., *Coatings.*, **2023**, *13*, 434.
33. Kokalj, A., *Corr. Sci.*, **2022**, *196*, 109939.
34. Kedimar, N.; Rao, P.; Rao, S. A., *Mater. Technol.*, **2023**, *38*(1), 2238414.
35. Murugan, K. S.; Mohanapriya, T., *Orient. J. Chem.*, **2022**, *38*(5), 1174-1182.
36. Budnyak, T. M.; Błachnio, M.; Slabon, A.; Jaworski, A.; Tertykh, V. A.; Deryło-Marczewska, A.; Marczewski, A. W., *J. Phys. Chem. C.*, **2020**, *124*, 15312–15323.
37. Hamza, R. A.; Samawi, K. A.; Salman, T. A., *Egypt. J. Chem.*, **2020**, *63*(8), 2863-2875.
38. Öztürk, T.; Gülfen, M.; Özdemir, A., *SN Appl. Sci.*, **2020**, *2*, 1886.
39. Feitosa, A. G.; Tatiane da Costa Santos, Y.; Menezes, J. M. C.; Coutinho, H. D. M.; Teixeira, V. F.; Hermínio da Silva, J.; José de Paula Filho, F.; Teixeira, R. N. P.; Oliveira, T. M. B. F., *Res. Chem.*, **2023**, *6*, 101205.
40. Go, L. C.; Depan, D.; Holmes, W. E.; Gallo, A.; Knierim, K.; Bertrand, T.; Hernandez, R., *PeerJ Mat. Sci.*, **2020**, *2*, e4.
41. Ogunyemi, B. T.; Latona, D. F.; Ayinde, A. A.; Adejoro, I. A., *Adv. J. Chem.-Sect. A.*, **2020**, *3*, 485–492.
42. Esan, T. O.; Oyeneyin, O. E.; Olanipekun, A. D.; Ipinloju, N., *Adv. J. Chem.-Section A.,* **2022**, *5*(4), 263-270.
43. Akbas, E.; Ruzgar, A., *Iran. J. Chem. Chem. Eng.*, **2022**, *41*, 1643–1656.
44. Hanoon, M. M.; Gbashi, Z. A.; Al-Amiery, A. A.; Kadhim, A.; Kadhum, A. A. H.; Takriff, M. S., *Prog. Color. Colorants Coat.*, **2022**, *15*, 133-141.
45. Bine, F. K.; Tasheh, S. N.; Nkungli, N. K; Ghogomu, J. N., *Comput. Chem.*, **2021**, *9*, 37-63.
46. Khabazi, M. E.; Chermahini, A. N., *A.C.S. Omega.*, **2023**, *8*, 9978–9994.
47. Oluwatoba, E. O.; Nathanael, D. O.; Nureni, I. E. B. A.; Abiodun, V. E., *Beni-Suef Univ. J. Basic Appl. Sci.*, **2022**, *11*, 132.
48. Diki, N.Y.S.; Coulibaly, N.H.; Kambiré, O.; Trokourey, A., *J. Mater. Sci. Chem. Eng.*, **2021**, *9*, 11-28.
49. Mrani, S. A.; Chihbi, E. E.; Arrousse, N.; Rais, Z.; El Hajjaji, F.; El Abiad, C.; Radi, S.; Mabrouki, J.; Taleb, M.; Jodeh, S., *Arab. J. Sci. Eng.*, **2021**, *46*, 5691–5707.
50. Tigori, M. A.; Koné, A.; Kouyaté, A.; Yeo, M.; Doumadé, Z.; Sissouma, D.; Niamien, P. M., *Int. J. Chem. Stud.*, **2022**, *10*, 111-124.
51. Zamindar, S.; Mandal, S.; Murmu, M.; Banerjee, P., *Mater. Adv.*, **2024**, *5*, 4563-4600.
52. Fouda, A. S.; Abdel Wahed, H. M.; Atia, M. F.; El Hossiany, A., *Sci. Rep.*, **2023**, *13*, 17593.
53. Chafiq, M.; Chaouikia, A.; Salghi, R.; Tachallait, H.; Bougrin, K.; Ali, I. H.; Siaj, M., *Chem. Phys.*, **2021**, *268*, 124742.
54. Desai, P. D.; Pawar, C. B.; Avhad, M. S.; More, A. P., *Vietnam J. Chem.*, **2023**, *61*(1), 15-42.
55. Gurjar, S.; Sharma, S. K.; Sharma, A.; Ratnani, S., *Electrochem. Sci. Adv.*, **2022**, *2*, e2100110.